Supplementary Information for

The 11-month precursory fault activation of the 2019 M_w 5.0 earthquake in the Weiyuan shale gas field, China

Jinping Zi[1†], Yuyun Yang[1†], Hongfeng Yang[1,2,3*], Jinrong Su[4]

[1]Earth and Environmental Sciences Programme, The Chinese University of Hong Kong, Shatin, Hong Kong
[2]Shenzhen Research Institute, The Chinese University of Hong Kong, Shenzhen, China
[3]Institute of Environment, Energy and Sustainability, The Chinese University of Hong Kong, Shatin, Hong Kong
[4]Earthquake Monitoring Center, Sichuan Earthquake Administration, Chengdu, China

*Corresponding author. Email: hyang@cuhk.edu.hk
[†]These authors contributed equally to this work

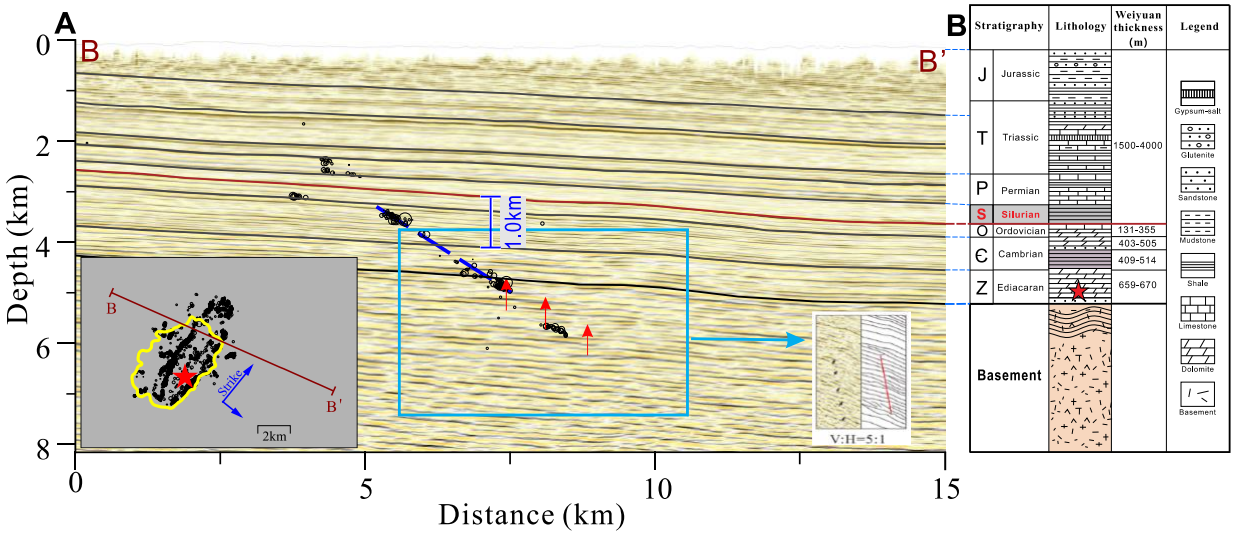

Fig. S1. Geological background in the M_w 5.0 hypocentral area. (A) Seismic reflection profile traverses the fault hosting the M_w 5.0 earthquake, with aftershocks within 1 km of the cross-section. The blue dashed line represents the fault fitted from aftershock distribution. Red arrows and the lower right inset denote the reported fault trace[23]. Lower left inset shows map view of the cross-section, the M_w 5.0 epicenter, the coseismic deformation area and aftershocks. (B) Modified synthetic strata column in the WSGF[27]. The Silurian shale-rich strata I, Cambrian shale-rich strata II and basement are colored. The hypocenter of the M_w 5.0 earthquake is placed 1.4 km below the target shale layer.

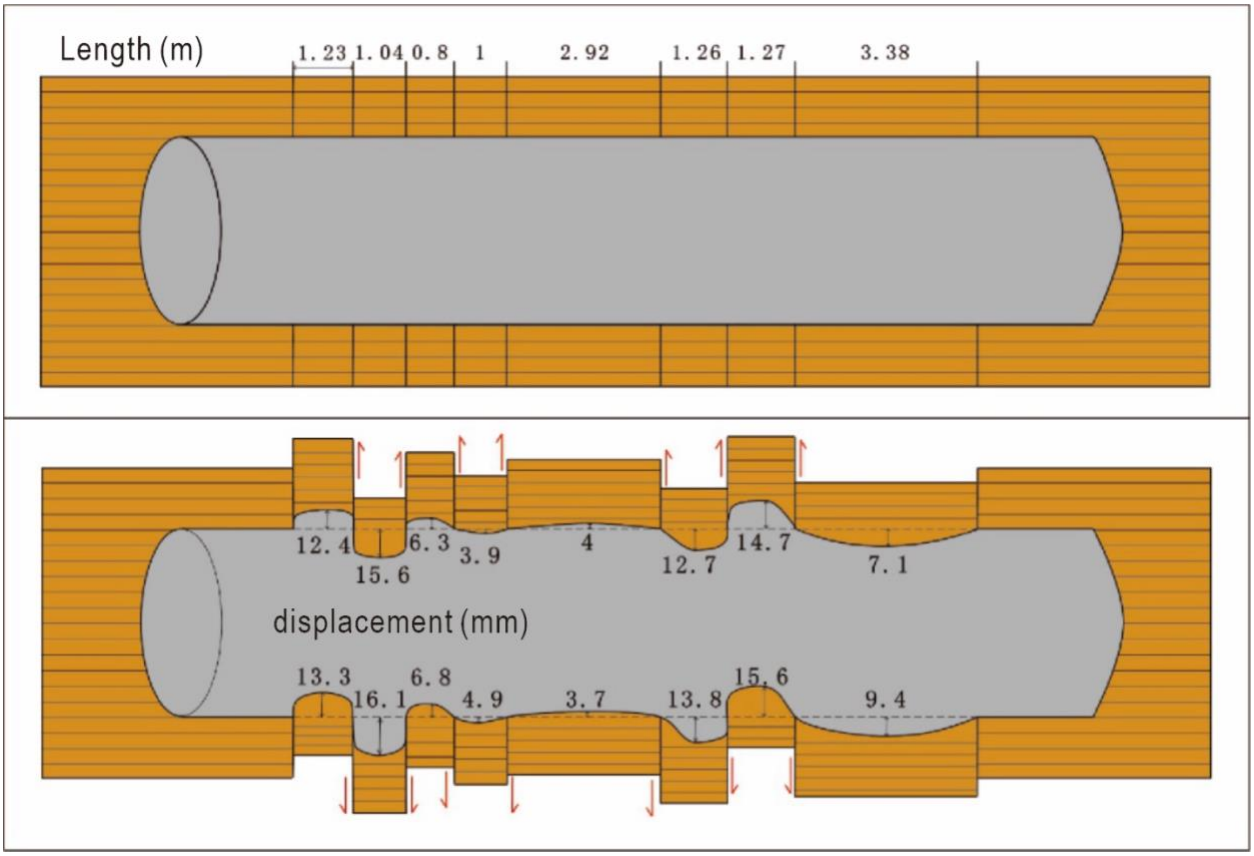

Fig. S2. Casing deformation in the H39 well pad. Map view of the reported casing deformation in one horizontal well of the H39 well pad[29] with maximum shear slip of 1.61 cm in a 12.9 m-long segment.

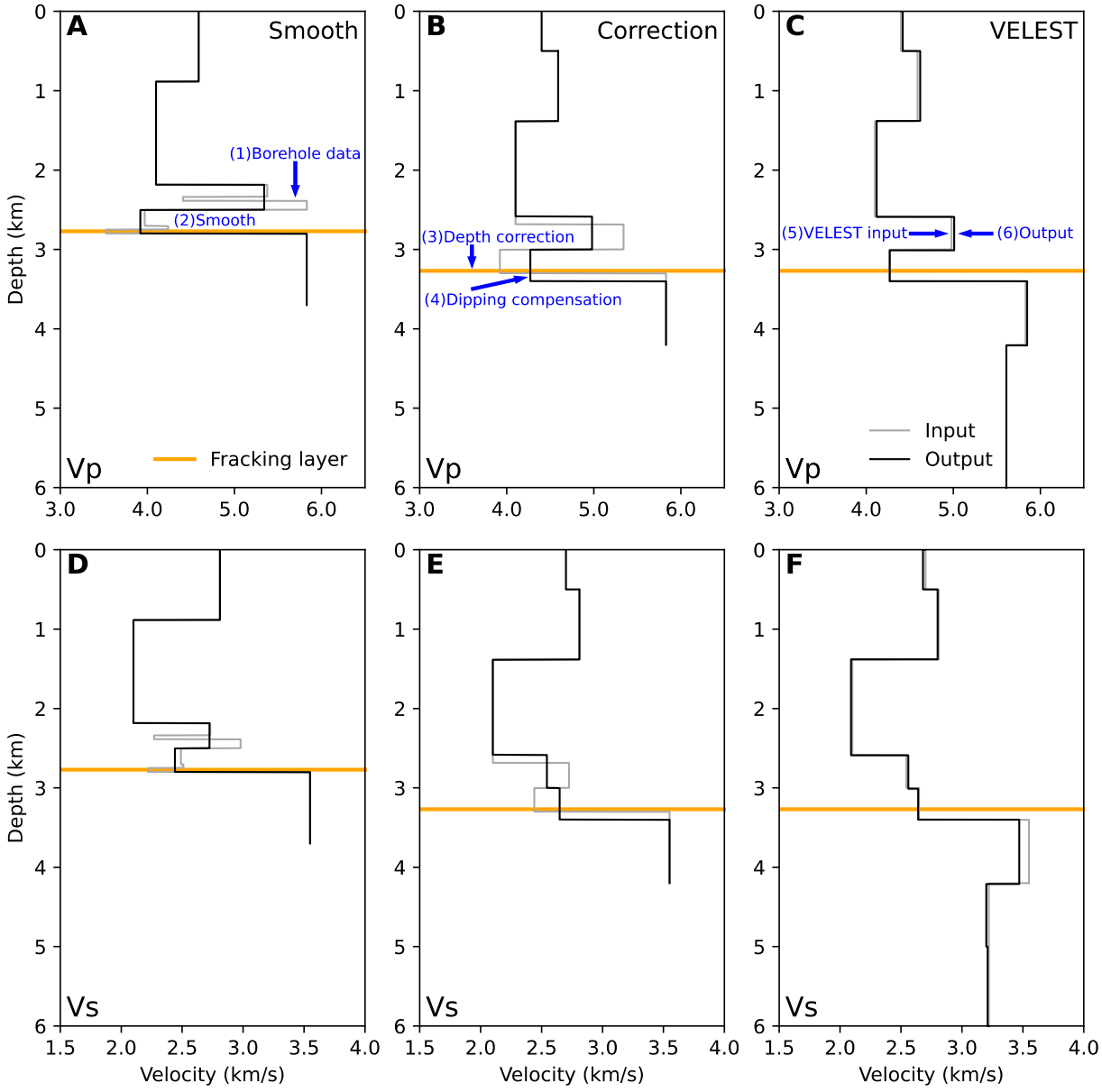

Fig. S3. Velocity model construction for V_p and V_s. (A, D) Original borehole measurements from a well 12.6 km from the M_w 5.0 epicenter (grey), and velocity models after smoothing the thin layers (black). (B, E) Velocity models after depth calibration according to buried depths of the target shale layer in the borehole and in the M_w 5.0 epicentral area (grey), and after extending the thicknesses of the target shale layer and the strata above it (black). (C, F) Input (grey) and output (black) of combined velocity models after VELEST inversion. The differences are minor.

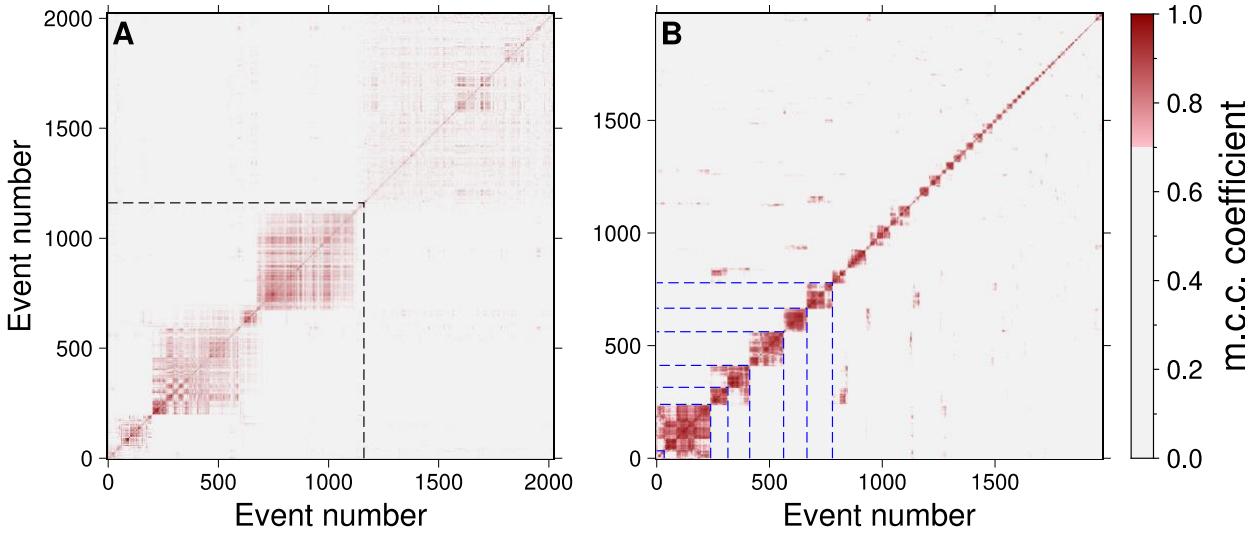

Fig. S4. Event similarity matrices in hierarchical clustering. (A) Waveform similarity matrix in chronological order. The black dashed line separates seismicity before and after the M_w 5.0 earthquake. (B) Event similarity matrix after level I hierarchical clustering. The dashed blue lines separate clusters, including 7 strong self-similar clusters and a weak self-similar cluster. m.c.c. coefficient: mean cross-correlation coefficient.

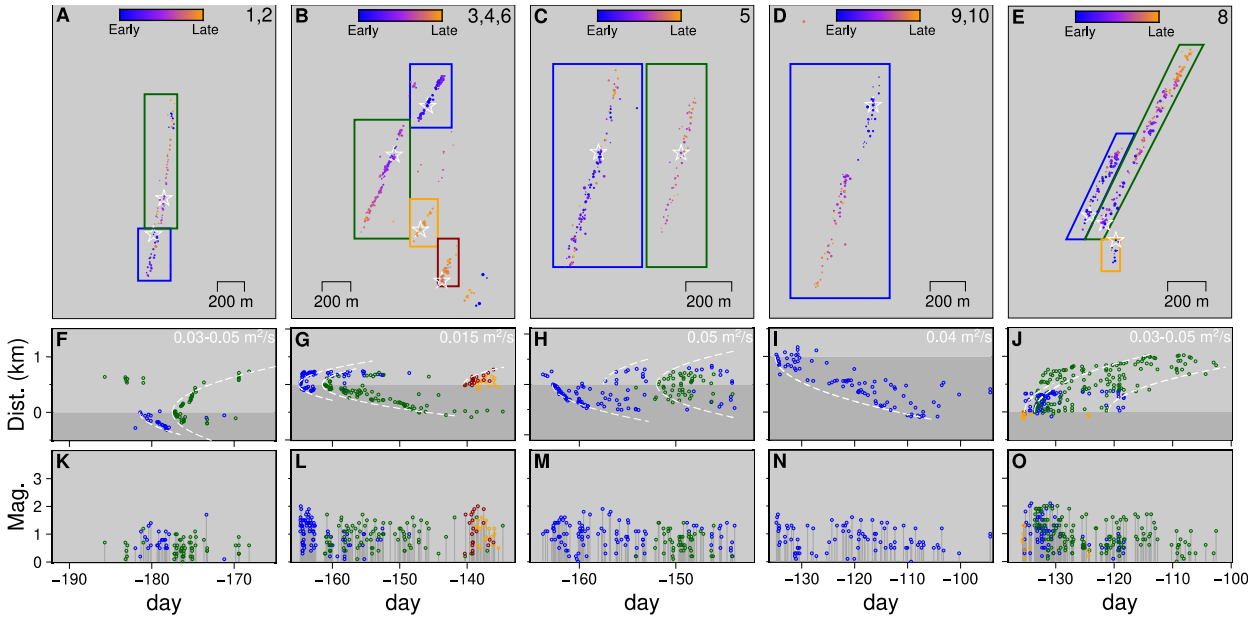

Fig. S5. Interpretation of the migration pattern of HF-induced clusters due to pore pressure diffusion. Cluster 7 has a limited number of earthquakes and is not plotted. (A–E) Map views of earthquakes in clusters with cluster ID(s) labeled in the upper right corner. Colored boxes enclose events for distance and magnitude vs. time plots below. White stars in the boxes are reference events for distance calculation. (F–J) Distance vs. time plots. The diffusion curve is plotted in white dashed lines, with the hydraulic diffusivity labeled in the upper right corner. (K–O) Magnitude vs. time plots.

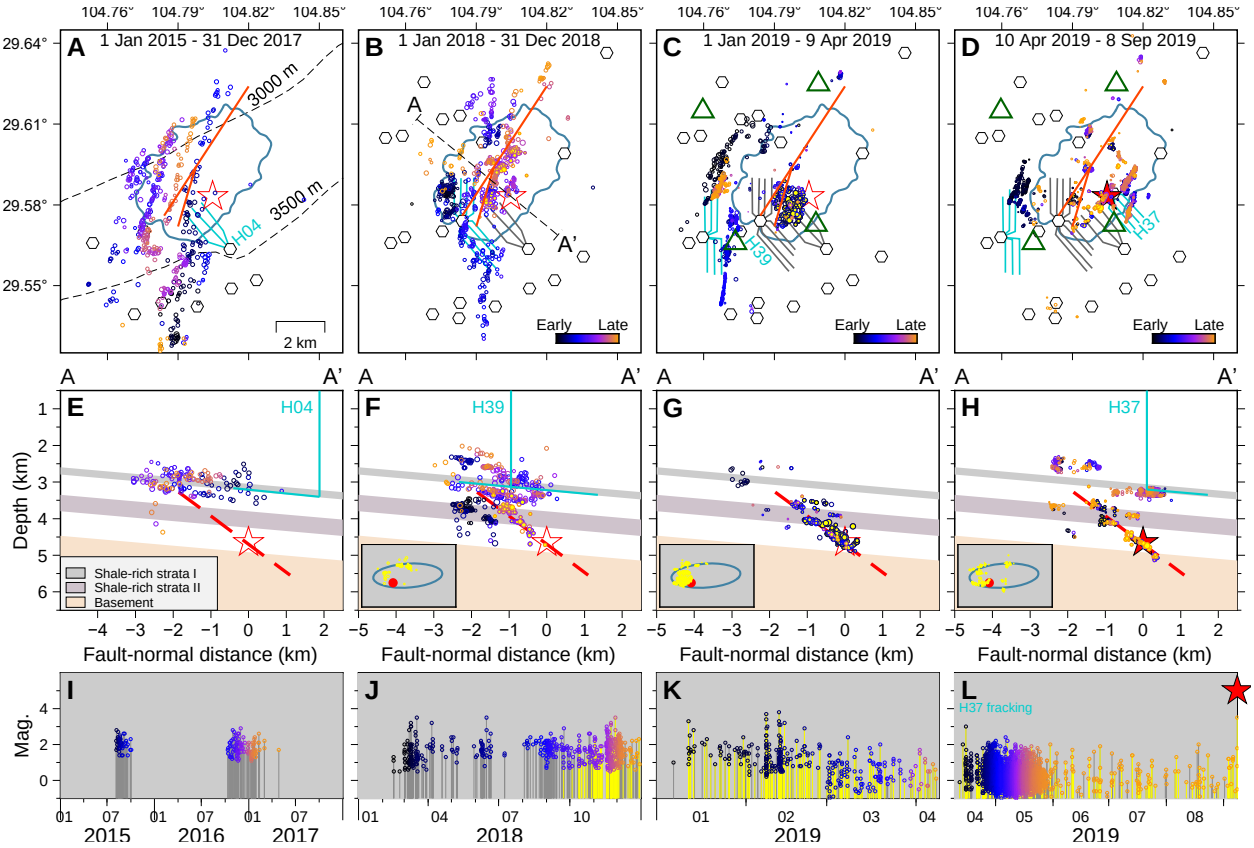

Fig. S6. Spatiotemporal distribution of earthquakes before the M_w 5.0 earthquake since 1 May 2015. Events are separated into four periods: from 1 January 2015 to 2017 (A, E, I), 2018 (B, F, J), 1 January 2019 to 9 April 2019 (C, G, K) and 10 April 2019 to 8 September 2019 (D, H, L). (A–D) Map views of earthquakes in the four periods with fault traces, coseismic deformation zone and horizontal wells. (E–H) Cross-section plots of earthquakes within the coseismic deformation zone. The red star and the red dashed line represent the M_w 5.0 hypocenter and the fault plane. On-fault earthquakes are filled in yellow. Insets are along-strike cross-section views of on-fault earthquakes and the M_w 5.0 earthquake. (I–L) Magnitude vs. time plots. Yellow lines mark on-fault earthquakes. Fracking period of the H37 well pad is highlighted in (L).

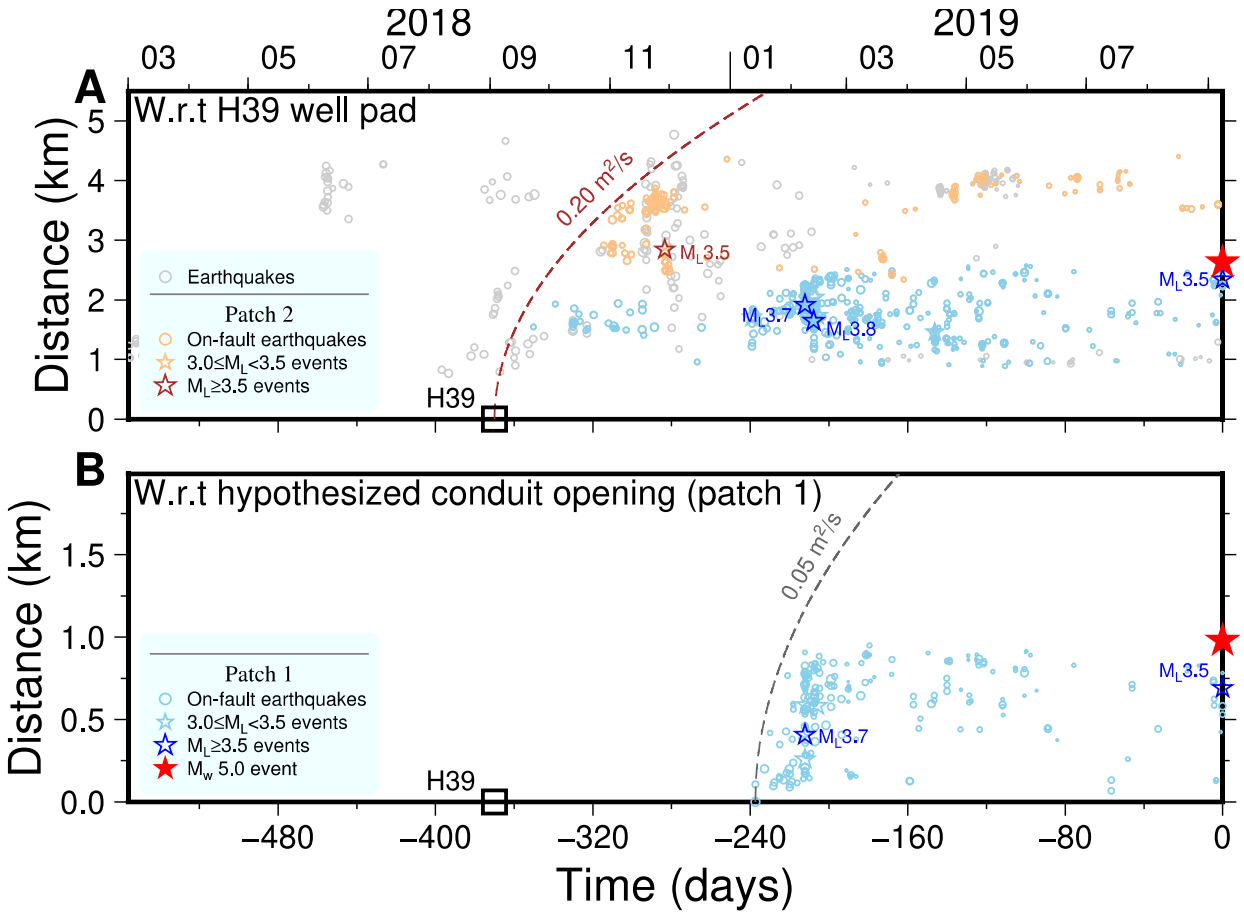

Fig. S7. Distance vs. time plots of earthquakes. (A) With reference to the H39 well pad. Gray circles are earthquakes that occurred within 0.5 km of the M_w 5.0 fault plane. Identified on-fault earthquakes on P1 & P2 are colored. A diffusion curve with a hydraulic diffusivity of 0.20 m^2/s is fitted. (B) On-fault earthquakes on P1, with reference to the event that marks activation of the deep segment of P1. A diffusion curve with a hydraulic diffusivity of 0.05 m^2/s is fitted.

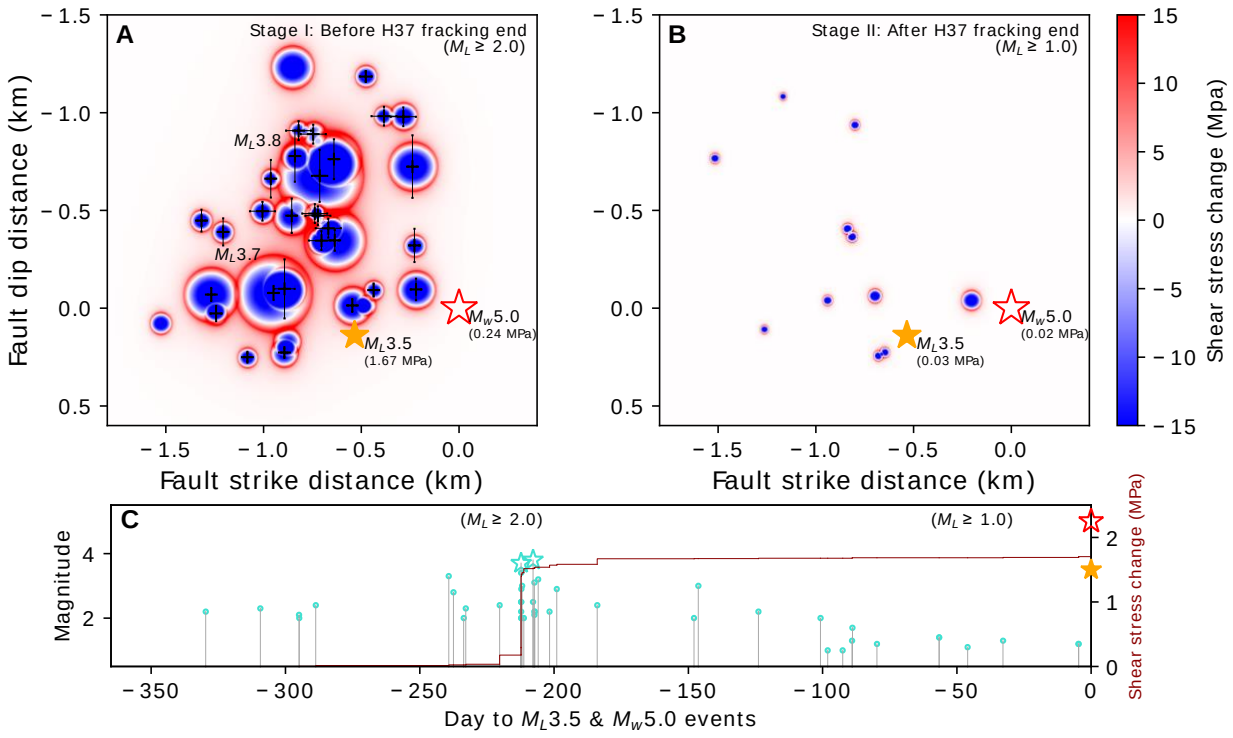

Fig. S8. Cumulative static shear stress change $\Delta\tau_s$ at the M_L 3.5 hypocenter (orange star) & M_w 5.0 hypocenter (red star). Location error bars of earthquakes with errors less than 20 m are not plotted. (A) $\Delta\tau_s$ from $M_L \geq 2.0$ events before the end of fracking at H37 (23 May 2019). (B) $\Delta\tau_s$ from $M_L \geq 1.0$ events after the end of fracking at H37. (C) Magnitude vs. time plot of events included in the estimation of $\Delta\tau_s$, and $\Delta\tau_s$ in dark red line.

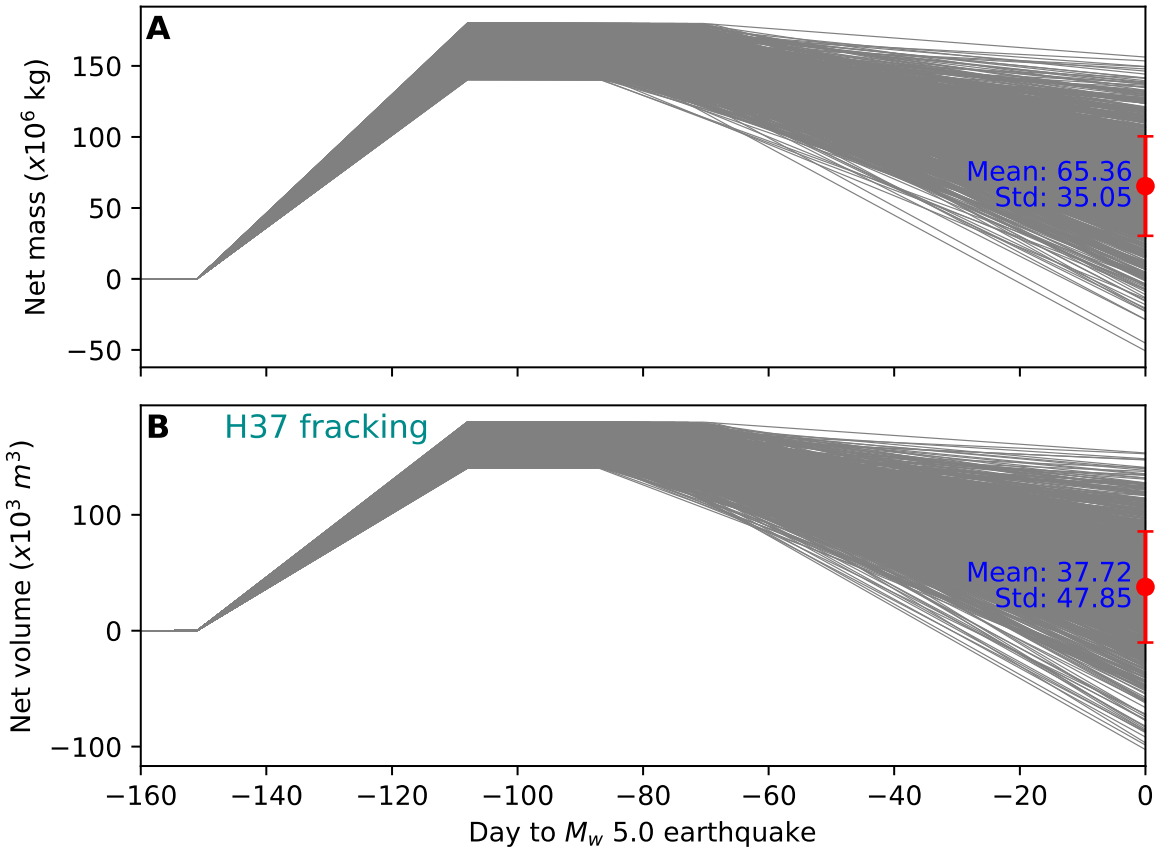

Fig. S9. Estimation of net injected mass and volume at H37. Bootstrap estimations were conducted 1,000 times. Mean and standard deviation are marked with red error bars.

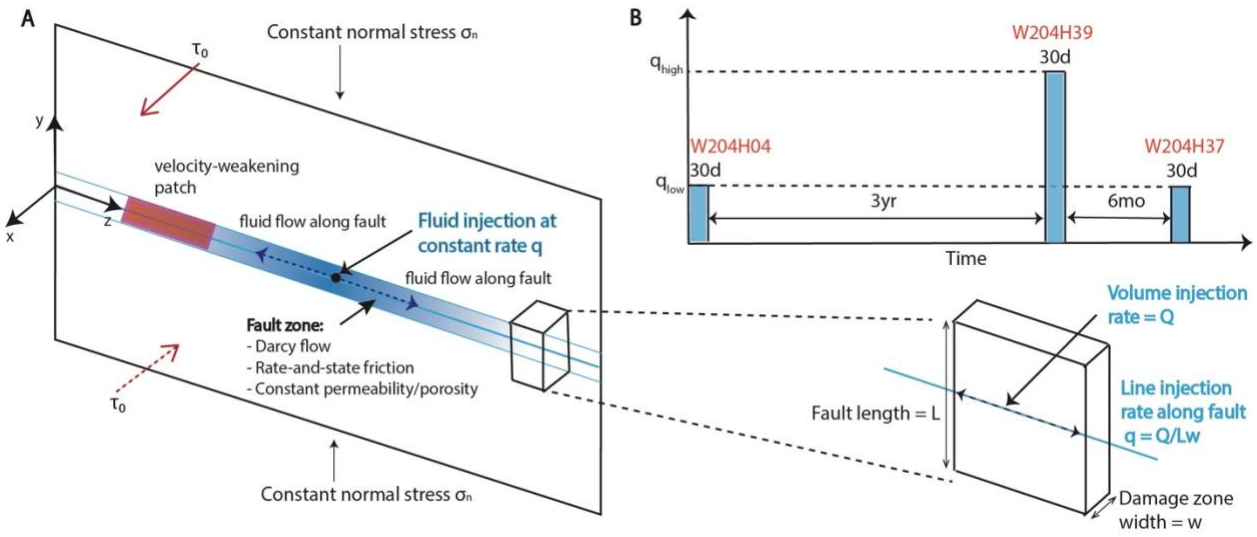

Fig. S10. Model setup for numerical simulation of injection into a fault. (A) The fault is in 2D antiplane shear, with constant normal stress σ_n and initial shear stress τ_0, obeying rate-and-state friction with the aging law. A VW patch is embedded in a VS fault some distance away from the injection point. Permeability and porosity are constant. Pore pressure diffuses along the fault following Darcy flow. Conversion from volume injection rate Q to line injection rate q is done via division by fault length L and damage zone width w. (B) Injection scheme for the three wells over time.

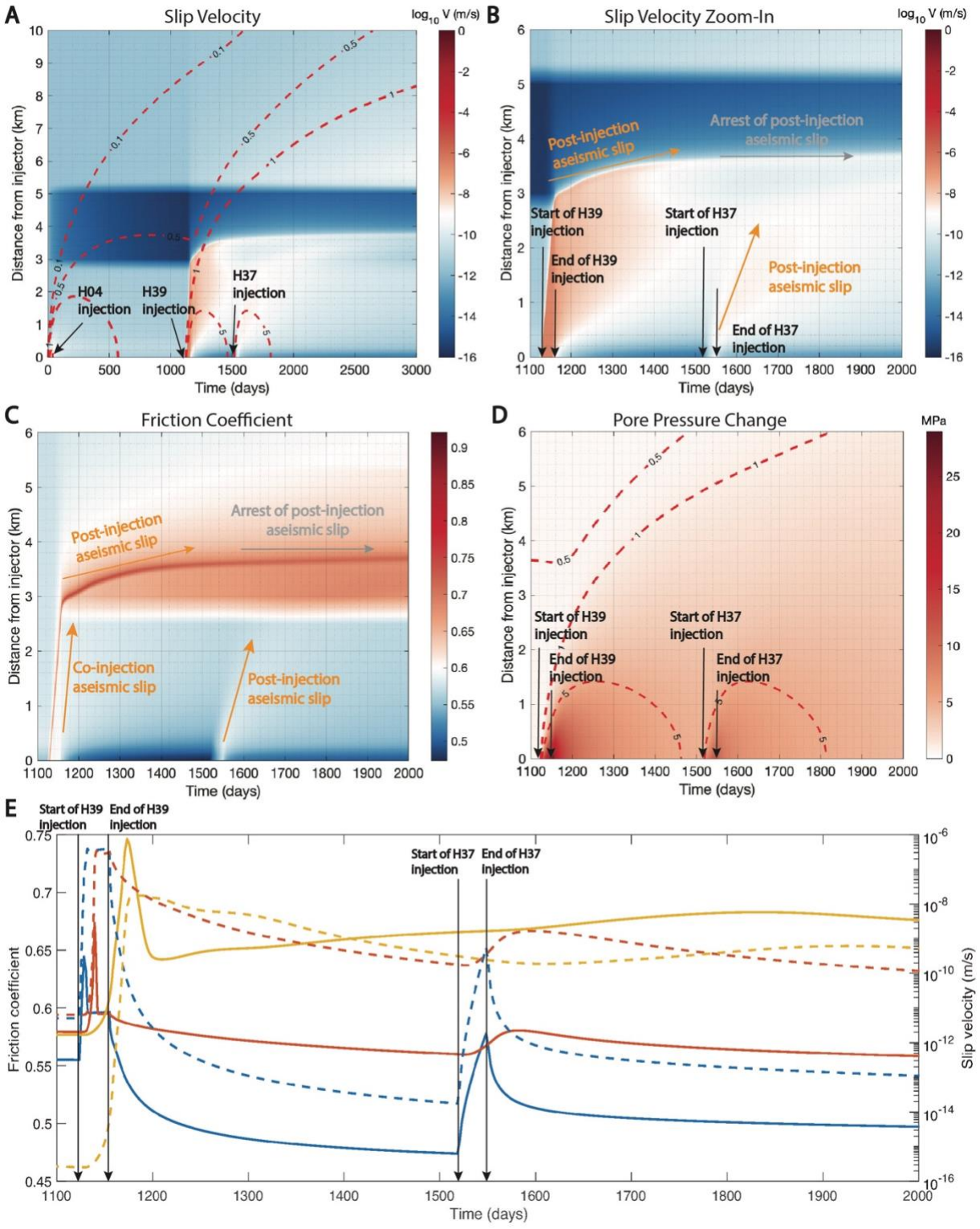

Fig. S11. Space-time plots of numerical simulation results if H39 and H37 injections were spaced 1 year apart. The same as Fig. 4 except for (C), where the space-time plot of friction coefficient is plotted. Note that post-injection aseismic slip arrests after the H37 injection and no earthquake is triggered in this case.

Period	I (1 Mar 2019 to 22 Sep 2019)	II (1 Jan 2015 to 28 Feb 2019)
Stations	6 (≤ 12 km)	6 (≤ 40 km)
Template quantity	329 ($M_L \geq 1.5$)	329 ($M_L \geq 1.5$)
Template length	4 s (-1 to 3 s w.r.t S-arrival)	6 s (-2 to 4 s w.r.t. S-arrival)
Initial detection	469,970	3,096,782
Positive criteria	S-wave similarity ≥ 0.7 on ≥ 3 stations	
Positive detection	9,303	742
Magnitude range (M_L)	-1.1 to 2.2	0.1 to 3.5
Grid-search space (x,y,z)	0.4 km × 0.4 km × 0.2 km	0.6 km × 0.6 km × 0.6 km

Table S1. Template matching setup and results. w.r.t.: with reference to.

Parameter	Value	Bootstrap distribution
Horizontal well quantity	4	-
Single-well injection volume (m^3)	35,000 – 45,000	uniform
Shut-in days	20 – 40	uniform
90-day flowback ratio	$\mu = 0.35$, $\sigma = 0.16$	normal
Free gas ratio	0.4 – 0.6	uniform
Production rate ($\times 10^4$ m^3/day)	$\mu = 21.3$, $\sigma = 12.81$	normal
Injection fluid density (ρ_f)	1000 kg/m^3	-
Gas density (ρ_g^n)	0.657 kg/m^3 (25°C, 1.01 bar)	-
Gas density (ρ_g^u)	306.91 kg/m^3 (89°C, 100 MPa)	-

Table S2. Parameters for the net injected mass and volume estimation. μ: mean, σ: standard deviation.

Symbol	Description	Value
μ	Shear modulus	32.4 GPa
σ_n	Fault normal stress	50 MPa
τ_0	Initial shear stress	28.5 MPa
f_0	Reference friction coefficient	0.6
V_0	Reference velocity	10^{-6} m/s
v_L	Plate loading velocity	10^{-12} m/s
a	Direct effect parameter	0.01
b	State evolution parameter	0.006 (VS), 0.02 (VW)
d_c	Characteristic state evolution distance	5 mm
Ψ_0	Initial state variable	0.7
q_{high}	Injection rate (H39)	10^{-5} m/s
q_{low}	Injection rate (H04, H37)	3×10^{-6} m/s
η	Fluid viscosity	10^{-3} Pa·s
β	Sum of elastic pore and fluid compressibility	10^{-8} Pa^{-1}
φ	Porosity	0.1
k	Permeability	10^{-13} m^2
L_y	Domain size in y direction	100 km
L_z	Domain size in z direction	100 km

Table S3. Reference parameters for numerical simulations. Most values are chosen to be consistent with those in previous studies[36,37].